

Contents:

- 1) Theoretical methods
- 2) Supporting results from static calculations
- 3) Supporting results from First Principles Molecular Dynamics (FPMD)
- 4) Supporting results on the molecule-surface coupling

1. THEORETICAL METHODS

We modeled the adsorption of gas-phase HCOOH on anatase $TiO_2(101)$ by both Density Functional Theory (DFT) structural optimizations (to obtain energy minima at 0 K) and First-Principles Molecular Dynamics (FPMD) simulations (to gather insight on the finite-temperature behavior of the system).^[1,2]

The adopted periodic slab ($Ti_{36}O_{72}$), formed by six Ti_6O_{12} layers (surface area: 10.349 × 11.355 Å²), provides a good description of the adsorption of probe molecules on $TiO_2(101)$ at both low- and high-coverage limits, as already demonstrated in previous studies.^[3–5] A vacuum region of 12 Å was adopted to minimize inter-slab interactions and the bottom Ti_6O_{12} atoms were held fixed. In most of the calculations, unless otherwise specified, the PBE approximation to DFT,^[6] plane-wave basis sets, and norm-conserving pseudopotentials were adopted, together with a non-linear core correction scheme for Ti (considered as Ti^{4+}).^[7–9] For the minimum structures described in the main text, additional geometry optimizations were performed with the PBE functional enhanced with dispersion corrections,^[10] and with the PBE0 hybrid functional.^[11]

In a preliminary set of geometry optimizations, different cutoff values were adopted to check convergence with respect to basis set truncation (see Table S1). As can be seen from data in Table S1, a planewave cutoff of 80 Ry already provided satisfactorily convergence for relative energies and binding energies of relevant surface adducts, and was therefore used in the production calculations. All calculations were performed at the Γ point, however convergence towards Brillouin Zone sampling was already tested in previous work.^[3]

A maximum force of 0.0005 Hartree/Bohr was used as convergence criterion for the forces on the ions in all geometry optimizations.^[12]

For all FPMD simulations, equations of motion were integrated with a time step of 3 au and a fictitious mass for electronic coefficients of 500 au. For each trajectory, data were collected for at least ~15 ps elapsed time, after 5 ps equilibration. In the equilibration runs, the systems were thermostatted at 300 K using Nose-Hoover chain thermostats.^[13,14] The thermostats were switched off in the production runs, which were then carried out in the NVE ensemble. These production room temperature FPMD simulations of HCOOH on top of TiO₂ were performed with a planewaves cutoff of 80Ry (320Ry for the electronic density). Such setup for FPMD simulations proved to be suitable for diverse complex organic-inorganic systems, including metal oxides, also containing Ti-sites.^[15–22]

Calculated IR signals were obtained via Fourier-transform of dipole-dipole autocorrelation functions. Instantaneous dipole moments were obtained via the (Γ -point) Berry Phase approximation.^[12] More specifically, the IR patterns for all the different configurations of HCOOH on the slab model were calculated by Fourier transform of dipole-dipole autocorrelation functions obtained from the respective FPMD trajectories. As common practice, in order to facilitate comparison with experimental spectra, a scaling factor was applied to the calculated spectra. The value of the scaling factor (1.0678) was obtained from the ratio of the highest wavenumbers' signals, i.e. the signals of the isolated surface hydroxyl group in the bridging HCOOH simulation and the experimental stretching value of isolated hydroxyl groups in anatase TiO₂ nanoparticles, as taken from Ref.^[23].

Also the adsorption of deuterated DCOOD on the $TiO_2(101)$ model slab was modeled via FPMD, adopting as initial configuration the one represented in Figure 1a. In this case, a production trajectory of 10 ps was performed, after 5 ps equilibration at 300 K.

In the case of the monodentate HCOOH on the $TiO_2(101)$ model slab (Figure 1a,e,f), the free energy for the acid-to-surface proton transfer was computed via a statistical sampling "bluemoon" approach.^[24] The reaction coordinate $r=r(H-O_s)-r(H-O_f)$ is defined as the difference between the distances of the proton from the carboxylate oxygen O_f and the surface oxygen O_s , respectively. The reaction coordinate was sampled by performing, along an interval of 0.82 Å, 12 FPMD simulations, by carrying out each simulation unless convergence of the constraint force was achieved. Two sets of bluemoon simulations were performed by thermostating the system at 50 K and 300 K, respectively.

From three relevant geometries extracted from the 50 K bluemoon sampling (*i.e.*, the two minima and the maximum in the free energy profile) we performed constrained geometry optimizations, using the same constraint adopted in the bluemoon sampling. The resulting optimized geometries correspond to the dissociated (I), undissociated (II) and proton-sharing (III) forms of the monodentate HCOOH adsorbate depicted in Figure 3 of the main text. Harmonic frequencies were then calculated on these three optimized geometries via a finite difference method. For the harmonic frequencies calculations, only the HCOOH atoms and the top TiO_2 layer were considered, all other TiO_2 atoms were fixed. Calculated frequencies obtained in such a way were all positive, and were adopted (unscaled) for the extimation of the zero point energy contributions for the three structures.

Graphical representations of the surface adducts have been created using the free molecular graphics program VMD^[25] (<u>http://www.ks.uiuc.edu/Research/vmd/</u>).

A full treatment of nuclear quantum effect, including tunnelling, would require methodologies, such as ab initio Path Integral Molecular Dynamics (PIMD).^[26,27] In this work, we considered the quantum effects for the HCOOH/TiO₂ system as essentially due to the zero point energy. Such an approximation might be justified on the basis of the following points:

- Tunnelling may be important for intramolecular proton transfer events in molecules with a rather stiff molecular skeletons, for example in thiotropolone,^[28] although the exact amount of tunnelling contribution to this reaction is still debated.^[28–30] In the case of HCOOH on TiO₂, proton transfer is not intermolecular but it occurs between the adsorbate and the surface. Reasonably, tunnelling effects, although not excluded, should not play a major part in the overall chemical picture of this process.

- Indeed, literature studies strongly suggest a net predominance of zero point energy effects for intermolecular and/or surface-mediated proton transfers. For example, comprehensive ab-initio PIMD studies on formic acid dimer evidence that for this system nuclear quantum effects are overwhelmingly due to zero-point motion effects.^[31] The dominant contribution of zero point energy to nuclear quantum effects has been highlighted also in a recent PIMD study of surface mediated water dissociation at finite temperature on metallic surfaces. It was found that the process has a negligible contribution from tunneling but is dominated by zero point energies.^[32]

2. SUPPORTING RESULTS FROM STATIC CALCULATIONS

2.1 Tests for Basis Set Convergenge (BSC) and adopted models

Table S1 reports the results of the plane-wave convergence tests for (PBE-DFT) calculations performed for four adsorption configurations of HCOOH on the $TiO_2(101)$ model slab depicted in Figure S1a-d. These four optimized geometries are relative to two molecularly adsorbed (Mol0, Mol1) and two dissociated (Bridge0, MonoDis) configurations, respectively. On the basis of these convergence tests, subsequent calculations were run with 80 Ry cutoff.

Table S1. Relative energies (in eV) with respect to the most stable structure of HCOOH adsorbed on TiO₂-anatase (101) as a function of basis set cutoff (BSC, in Ry). The binding energy (in eV) is reported in parenthesis.

BSC	Mol0	Mol1	Bridge0	MonoDis
80	0.0 (0.971)	0.011 (0.960)	0.042 (0.929)	0.598 (0.373)
90	0.0 (0.952)	0.008 (0.944)	0.030 (0.922)	0.576 (0.375)
100	0.0 (0.941)	0.010 (0.931)	0.033 (0.907)	0.576 (0.363)
120	0.0 (0.947)	0.010 (0.937)	0.034 (0.912)	0.577 (0.369)
140	0.0 (0.947)	0.008 (0.939)	0.031 (0.916)	0.575 (0.372)
160	0.0 (0.941)	0.008 (0.933)	0.034 (0.907)	0.575 (0.366)

We decided to focus on the fully oxidized non-defected TiO_2 anatase (101)-surface because, in spite of being the most stable TiO_2 anatase facet, it displayed most clearly the unsolved fundamental problem that attracted our attention: the location of the acid proton. Moreover, it can be considered as a reference in TiO_2 surface science: previous static calculations on anatase-TiO₂ were performed mostly on regular (101) surfaces, and more accurate experimental structural data were available for this system.

In non-stoichiometric reduced anatase, IRRAS data suggest a different anchoring of HCOOH with respect to stoichiometric non defective (101) anatase.^[33] On the other hand, stoichiometric anatase nanoparticles are mainly terminated by (101) facets, with defects mainly localized at edges and corners.^[34,35] Moreover, it has been shown that aminoacid reactivity is not dependent on the presence of defects on different (101)-terminated anatase nanoparticles characterized by different morphology and defects concentration.^[36] We therefore can conclude that the main issue tackled in this manuscript can be transferred also to stoichiometric nanoparticles whose terminations are mainly (101) ones.

Particular attention was devoted to structure MonoDis (1d, see also main text), represented in Figure S1d, which features a dissociated monodentate formate whose (dissociated) acid proton is not hydrogen-bonded with the formate. For this system, we calculated the harmonic frequencies via a finite differences approach at the PBE 80 Ry level of theory. The frequency associated to the OH stretching mode was 3621 cm⁻¹. Therefore, we excluded this strucure from further analysis because in the IRRAS experiment no signal in the region typical of the OH stretching mode (i.e. > 3000 cm^{-1}) was detected.

Importantly, this adduct is also thermally unstable: after few ps of FPMD at 300 K, the adduct in Figure S1d relaxed to a structure close to the one represented in Figure S1b. This behaviour

can be understood by observing that MonoDis is considerably higher in energy than the other three adducts in Table S1.

Essentially, the MonoDis model was an attempt to mimick dissociated monodentate formate – i.e. the most probable adsorption geometry deduced by IRRAS data on regular, fully-oxidized anatase-TiO₂(101) single crystal surfaces.^[33] In order to ensure electroneutrality, a proton had to be included in this model as well. However, the available IRRAS and STM experiments did not provide specific information on the position of the dissociated acid proton.^[33,37] For this reason, in the starting configuration for the FPMD simulation of the MonoDis model, we arbitrarily positioned the acid proton on an oxygen site not directly bonded to the Ti adsorption site, as depicted in Figure S1d. The reason for this choice was that monodentate dissociated formate with the proton located on a nearby oxygen site was unstable during optimization and, upon rotation around the Ti-O bond, it rapidly evolved to a structure stabilized by a short hydrogen bond, like that reported in Figure S1f.

To deepen our analysis, we searched for alternative locations of the acid proton compatible with dissociated monodentate formate. In particular, we considered the possibility that the acid proton could be found in a subsurface location, forming a subsurface -OH- moiety bonded to two neighboring Ti cations. Our reasoning was that a subsurface proton should be, very likely, practically invisible to the STM tip, and hence able to escape experimental detection via this technique. Hence, we built a new model of the surface featuring a subsurface -OH group (Figure S1g), and optimized its structure in order to calculate the harmonic frequencies. During optimization, the monodentate dissocated formate evolved towards a more stable minimum of the potential energy surface, i.e. bridiging bidentate (Figure S1h,i). Such a minimum, however, is higher in energy than molecular monodentate Mol0 ($\Delta E= 3.77$ kcal/mol). Vibrational analysis indicated that the subsurface -OH group has a harmonic stretching frequency at 3471 cm⁻¹ i.e. well outside the region of short strong hydrogen bonds. Hence, if a subsurface -OH moiety were present, it should likely be detectable by means of vibrational spectroscopy. However, no experimental IR features were detected around 3400-3500 cm⁻¹. On the basis of these results, we may safely rule out, at least on regular anatase (101) surfaces, the positioning of the acid proton in a subsurface location because:

- The subsurface proton would be stably bonded to a single oxygen site, forming an –OH moiety resonating at 3400-3500 cm⁻¹ (which should be detactable by vibrational spectroscopy);
- Formation of subsurface –OH would be accompanied by formation of bridging bidentate formate, excluded on the basis of IRRAS data (see ref.^[33])

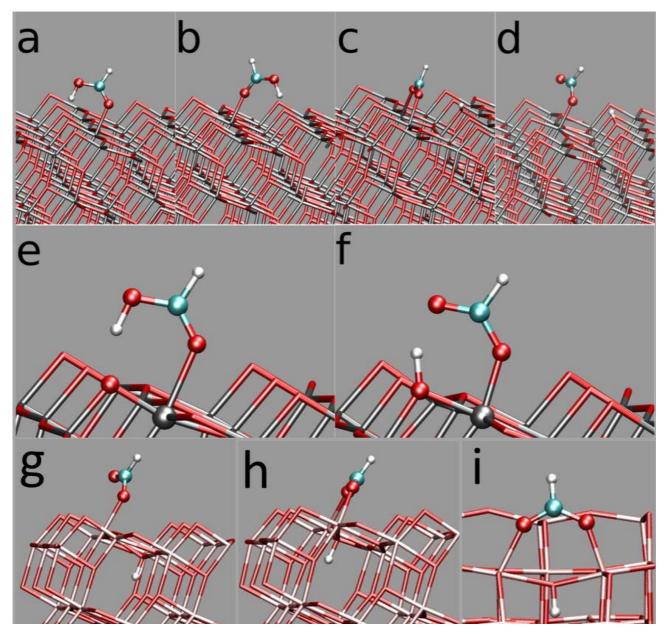


Figure S1. a-d): Optimized structures of HCOOH on anatase-TiO₂ (101). **a)**: Mol0, **b)**:Mol1, **c)**:Bridge0, **d)**:MonoDis. **e,f)**: Snapshots from the 300 K trajectory of formic acid on anatase-TiO₂(101). **e)**: molecularly adsorbed HCOOH; **f)**: dissociatively adsorbed HCOOH. **g-i)**: alternative adsorption models for dissociated formate, with the acid proton located in the subsurface layer, forming an OH moiety bonded to two neighboring Ti cations. g): monodentate dissociated formate and subsurface OH; h) bridging bidentate formate and subsurface OH (side view); i) bridging bidentate formate and subsurface OH (side view); i) bridging bidentate formate and subsurface OH (front view). Atom colors: red=O; gray=Ti; cyan=C; white=H.

2.2 Bader analysis

The Bader atomic charges^[38,39] computed for gas-phase HCOOH, for the proton-sharing surface adduct (form **III**, Figure 3) and for the Bridge0 structure (all optimized at the PBE level) are reported in Table S2. Bader charges were calculated from the total electronic density obtained with PAW pseudopotentials,^[40] that allows the reconstruction of the core density. Wavefunctions cutoff in this case was 40 Ry, while the cutoff for the density representation was

320 Ry. PAW calculations were performed with the PWscf code of the Quantum espresso package.^[41] The total electronic density was represented on a dense grid, giving an estimated accuracy of ± 0.005 electrons (estimated from the total charge of isolated HCOOH). Atomic charges were calculated with the Bader program developed by the Henkelman group^[42–44] (http://theory.cm.utexas.edu/henkelman/code/bader).

Table S2. Bader atomic charges (in e units) for HCOOH in the gas phase and on top of $TiO_2(101)$ anatase. Total charges are calculated as the sum of the individual atomic contributions. The total charge relative to the Bridge0 structure refers to the adsorbed formate moiety.

	gas-HCOOH	Proton sharing (III)	Bridge0
O _(C=0)	-1.098517	-1.119315	-1.148665
О _(О-Н)	-1.125312	-1.145178	-1.157852
С	1.496807	1.561371	1.581435
$\mathbf{H}_{(C-H)}$	0.106126	0.096514	0.088352
H _(acid proton)	0.616055	0.626897	0.634349
Total	-0.005	0.020	-0.637

The data in the table clearly show that the proton-sharing structure **III** of adsorbed formic acid, which can be considered a single entity, is a neutral species, while the bridging adsorption mode of HCOOH implies the formation of a negatively charged moiety plus a separated adsorbed proton.

3 SUPPORTING RESULTS FROM FPMD SIMULATIONS

3.1 Structure of the initial and final state of the free energy profile

Relevant average geometrical parameters from the Bluemoon-enhanced FPMD simulations for the Initial and Final state of the free energy profile (Figure S2) are reported in Table S3.

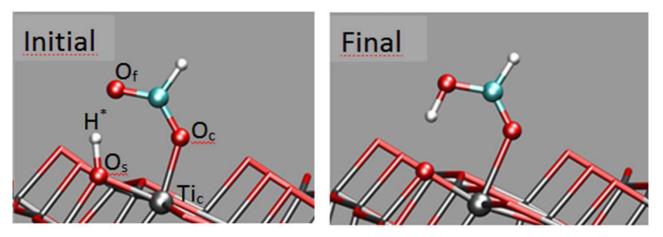


Figure S2. Graphical representation of the initial and final states of the free energy profile. Atom colors: red=O; gray=Ti; cyan=C; white=H.

Distance (Å)	Initial 50 K	Final 50 K	Initial 300 K	final 300 K
O _f -O _s	2.460±0.018	2.480 ± 0.024	2.487±0.052	2.517±0.056
О _г - Н*	1.436 ± 0.009	1.064 ± 0.012	1.492 ± 0.030	1.048 ± 0.029
H*-O _s	1.065 ± 0.009	1.445 ± 0.012	1.055 ± 0.030	1.519 ± 0.029
O _s -Ti _c	1.959 ± 0.020	1.910 ± 0.021	1.970 ± 0.045	1.909 ± 0.053
O _c -Ti _c	1.985 ± 0.020	2.111 ± 0.028	1.989 ± 0.056	2.155 ± 0.079
O _c -C	1.289 ± 0.010	1.246 ± 0.009	1.294 ± 0.024	1.244 ± 0.021
O _f -C	1.249 ± 0.009	1.295 ± 0.010	1.248 ± 0.021	1.304 ± 0.026
Angles (°)				
O _c -Ti _c O _s	84.17±1.22	85.45±1.17	84.36±2.62	84.41±3.23
O _c -C –O _f	125.90±1.15	125.89±1.23	125.73±2.94	125.85±2.85

Table S3. Average geometrical parameters from FPMD (Labels as in Fig. S2).

We recall that the standard deviations in Table S3 should be interpreted as an estimate of the thermal fluctuations of the corresponding geometrical variable. As can be seen, apart from the thermal fluctuations (which, as expected, are significantly greater at 300 K), the average geometrical parameters characterizing the HCOOH-TiO₂ moiety in the initial and in the final configuration of the free energy profile (shown in Figure 3 of the main text) do not significantly change in passing from 50 K to 300 K. It is however clear that, as temperature raises, the adsorbed molecule slightly increases its separation from the surface.

3.2 Simulated IR patterns

Whereas in the main text we discussed only the results obtained with PBE for a 300 K FPMD simulation for monodentate HCOOH, and for a 300 K simulation of bridging bidentate formate, other simulations were performed.

As regards the 300 K simulations, two independent FPMD simulations with different starting configurations were performed for each adsorption mode. In two FPMD's, an undissociated HCOOH was positioned on top of the $TiO_2(101)$ slab model in different configurations corresponding to the "monodentate" mode (Figure S1a, S1b) while in two other FPMD's a formate (HCOO-) moiety was located on top of a protonated slab model in bidentate "bridging" mode (Bridge0: Figure S1c and Figure S3a; Bridge1: Figure S3b).

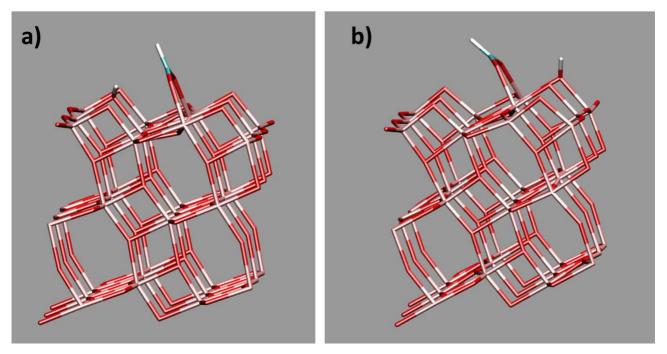


Figure S3. Graphical representations of the Bridge0 (**a**) and Bridge1 (**b**) models of dissociate bidentate bridging formate. The two structures differ for the position of the protons. Atom colors: red=O; gray=Ti; cyan=C; white=H.

The simulated IR patterns from the sets of trajectories for monodentate HCOOH and bridging HCOOH are compared in Figure S4. It can clearly be seen that the signal of the hydroxyl group (at wawenumbers $> 3500 \text{ cm}^{-1}$) is present only for the "bridging" cases and missing for the monodentate HCOOH (Mol0 and Mol1).

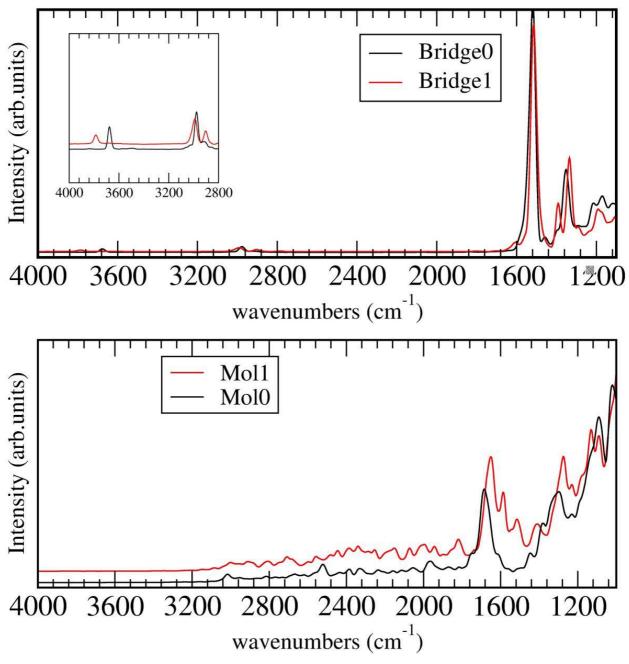


Figure S4. Simulated IR spectra from fourier-transforms of the autocorrelation functions of the dipole moment components. Top: IR spectra for HCOOH in the "bridging" adsorption mode (Inset: zoomed view of the high-wavenumber region). Bottom: IR spectra for HCOOH in the undissociated monodentate adsorption mode.

3.3 Simulation of deuterated formic acid (DCOOD) on $TiO_2(101)$

To shed more light on the molecule-surface proton shuttling emerged from the 300 K simulations on monodentate HCOOH, we investigated the effect of the proton/deuteron substitution by considering the adsorption of DCOOD on the same slab.

The 300 K trajectory of monodentate DCOOD on $TiO_2(101)$ provided very similar results to the corresponding simulation relative to HCOOH. In particular, both the 300 K simulations, performed either with DCOOD or HCOOH, revealed that the acid proton shuttles between a TiO_2 surface oxygen (O_s) and the carboxylic oxygen O_f indicating a fast equilibrium between formic acid and formate on the anatase $TiO_2(101)$ surface. For example, by inspecting the time evolution of the H-O distances relative to O_s and O_f in HCOOH and of the D-O distances in DCOOD (Figure S5), it is clear that the proton (the deuteron in the DCOOD case) frequently changes its bonding partner during a time frame of 10 ps along the trajectory.

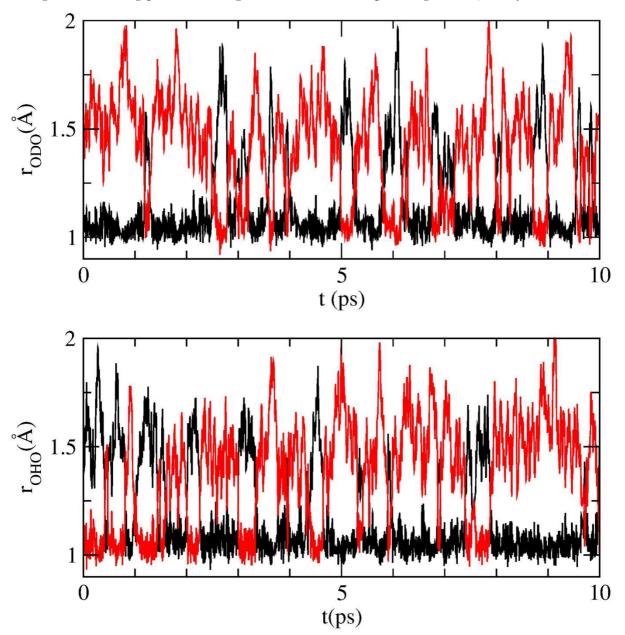


Figure S5. Comparison of the time evolution of the D-O (top panel) and H-O distances (bottom panel) relative to O_f and O_s (black and red lines, respectively) obtained from the 300 K simulation of DCOOD and HCOOH, respectively, on the anatase TiO₂(101) slab.

1. SUPPORTING RESULTS on MOLECULE-SURFACE COUPLING

Short-strong hydrogen bonds (SSHB) in the solid phase are characterized by short distances and significant electron-density sharing between the donor (D) and acceptor (A) atoms (around 2.5 A), giving thus the SSHB a weakly covalent character. Indeed, the D-H-A moiety is often described as a three-center-four electron bond. Moreover, previous experimental and theoretical studies have shown that proton migration between donor and acceptor atoms in crystalline systems such as e.g. dimethylurea–oxalic acid^[45] and dymethilurea-phosphoric acid,^[46,47] depends on low-frequency phonons. In SSHB in crystalline systems, the proton is therefore coupled both electronically and vibrationally to the lattice.

Our heterogeneous system, comprising a gas-phase HCOOH molecule interacting with anatase TiO_2 (101) surface, is characterized by a SSHB manifesting the above-described features, typical of SSHBs in crystalline environments: namely, the "floating" proton is coupled both electronically and vibrationally to the anatase surface.

Surface-molecule electronic coupling can be visually sketched by the three molecular orbitals mostly involving the shared proton (Figure S6) calculated for the surface adducts **I**, **II**, **III**. These pictures clearly evidence the sharing of electron density in the SSHB between HCOOH and TiO_2 . Significantly, electron density sharing is operative not only for the shared-proton form (**III**), but also for the energy minima related to the initial (**I**) and final (**II**) states of the free energy profile.

The partially covalent character of the SSHB in the shared proton form (III) can be visually appreciated also from the Bader volumes associated to the shared proton, the TiO_2 surface oxygen (O_s) and the carboxylic oxygen O_f (Figure S7). According to the Quantum Theory of Atoms In Molecules (QTAIM),^[39] each Bader volume (or atomic basin) contains a single electronic density maximum and is delimited by a zero-flux surface of the electron density, on which the normal component of the gradient of the electron density is zero. Such zero-flux surfaces partition the molecular space into separate atomic basins and are characteristic of bonding interactions.^[48] Figure S7 clearly shows that the Bader volume associated to the shared proton shares a common interatomic zero-flux surface of the electronic density with both the O_s and O_f atoms, thus further highlighting the electronic coupling of the proton with both the adsorbate and the surface.

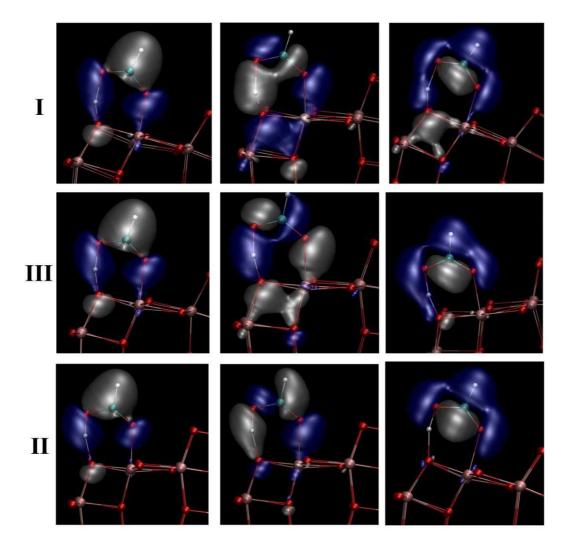


Figure S6. Graphical representation of three significant Kohn-Sham molecular orbitals relative to the bonding of HCOOH to TiO₂-anatase (101) for structures **I** (top), **III** (middle), **II** (bottom). Blue and white regions represent positive and negative lobes, respectively. Atom colors: red=O; pink=Ti; cyan=C; white=H.

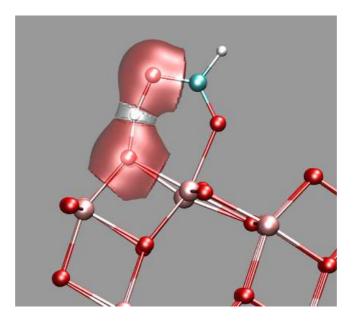


Figure S7. Bader volumes associated to the O_f and O_s atoms (red) and to the shared proton (white) for structure **III** (isodensity contour used for the picture = 0.04 e/Å³). Atom colors: red=O; pink=Ti; cyan=C; white=H.

The vibrational coupling between HCOOH and TiO_2 was investigated by computing partial vibrational density of states for selected atoms/groups of atoms. The partial vibrational densities of states (also known as partial power spectra) shown in Figure S8 were obtained by fourier-transforming the velocity-velocity autocorrelation functions calculated for selected atoms/groups of atoms along the 300 K FPMD trajectory of monodentate HCOOH.

Indeed the partial power spectrum of H in the 0-1000 cm⁻¹ interval shows a number of features which are present also in the partial power spectra of the slab atoms. In particular, by considering the partial spectrum of Ti_c-O_s atoms - i.e. the surface atoms directly bonded to HCOOH (see Figure S2), overlapping bands are found at circa 750 and 660 cm⁻¹, along with a signal at very low wavenumbers (about 25 cm⁻¹), and a number of features in the 50-350 cm⁻¹ interval (Figure S8a). The coupling is even more evident by considering the superpositions of the H partial spectrum with the partial spectra of the individual Ti_c and O_s atoms (Figure S8b). This result can be easily understood by considering that O_s is directly involved in the SSHB, and that T_c is bonded to the second carboxyl oxygen (Figure S2). Nonetheless, note that the surface-molecule coupling involve also the inner atoms of the TiO₂ slab (which are not directly bonded to the adsorbate): in particular, in addition to the already described bands, the power spectra of the sub-surface Ti and O atoms closest to the shared proton exhibit another signal at circa 780 cm⁻¹ which overlaps with the power spectra of the shared proton (Figure S8c). Furthermore, the power spectrum of all TiO₂ slab atoms has a new overlapping feature at about 850 cm⁻¹ (Figure S8d). These results indicate therefore, that the (anharmonic) vibrational modes of the slab are coupled to the proton modes, and suggests that the thermal fluctuations of the SSHB environment - which can be associated to room-temperature proton shuttling, are likely promoted by TiO₂ lattice vibrations.

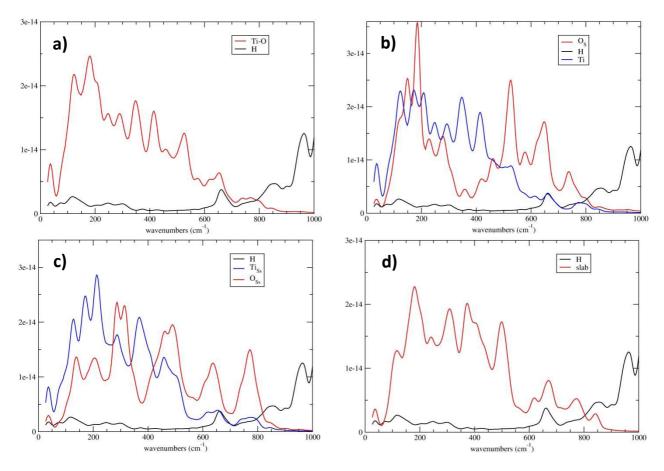


Figure S8. Partial vibrational density of states (power spectra) calculated from the 300K FPMD trajectory of monodentate HCOOH. **a**): Power spectra of the shared proton (black) and of the Ti_c -O_s atoms (red) (See Figure S2 for labels); **b**) Power spectra of the shared proton (black), of the Ti_c atom (blue), and of the O_s atom (red); **c**) Power spectra of the shared proton (black), and of the closest sub-surface atoms Ti_{Ss} (blue) and O_{Ss} (red); **d**) Power spectra of the shared proton (black), and of all the TiO₂-slab atoms (red). The (unscaled) spectra are shown in the interval 0-1000 cm⁻¹, where TiO₂ vibrations are found.

References

- [1] R. Car, M. Parrinello, Phys. Rev. Lett. 1985, 55, 2471–2474.
- [2] IBM Corp. 1990–2017, MPI für Festkörperforschung Stuttgart 1997–2001, 2017.
- [3] C. Deiana, M. Minella, G. Tabacchi, V. Maurino, E. Fois, G. Martra, *Phys. Chem. Chem. Phys.* 2013, 15, 307–15.
- [4] C. Deiana, G. Tabacchi, V. Maurino, S. Coluccia, G. Martra, E. Fois, *Phys. Chem. Chem. Phys.* **2013**, *15*, 13391–13399.
- [5] C. Deiana, E. Fois, G. Martra, S. Narbey, F. Pellegrino, G. Tabacchi, *ChemPhysChem* 2016, 17, 1956–1960.
- [6] J. P. Perdew, K. Burke, M. Ernzerhof, Phys. Rev. Lett. 1996, 77, 3865–3868.
- [7] N. Troullier, J. L. Martins, *Phys. Rev. B* 1991, 43, 1993–2006.
- [8] D. Hamann, M. Schlüter, C. Chiang, Phys. Rev. Lett. 1979, 43, 1494–1497.
- [9] L. Kleinman, D. M. Bylander, *Phys. Rev. Lett.* **1982**, *48*, 1425–1428.
- [10] S. Grimme, J. Comput. Chem. 2006, 27, 1787–1799.
- [11] C. Adamo, V. Barone, J. Chem. Phys. 1999, 110, 6158–6170.

- [12] D. Marx, J. Hutter, *Ab Initio Molecular Dynamics*, Cambridge University Press, Cambridge, 2009.
- [13] S. Nosé, J. Chem. Phys. 1984, 81, 511–519.
- [14] W. G. Hoover, Phys. Rev. A 1985, 31, 1695–1697.
- [15] E. Fois, A. Gamba, G. Tabacchi, *Chemphyschem* **2005**, *6*, 1237–9.
- [16] A. Gamba, G. Tabacchi, E. Fois, J. Phys. Chem. A 2009, 113, 15006–15015.
- [17] E. Fois, A. Gamba, G. Tabacchi, ChemPhysChem 2008, 9, 538–543.
- [18] E. Spanó, G. Tabacchi, A. Gamba, E. Fois, J. Phys. Chem. B 2006, 110, 21651-21661.
- [19] G. Tabacchi, E. Gianotti, E. Fois, G. Martra, L. Marchese, S. Coluccia, A. Gamba, J. Phys. Chem. C 2007, 111, 4946–4955.
- [20] E. Fois, G. Tabacchi, D. Barreca, A. Gasparotto, E. Tondello, Angew. Chemie 2010, 122, 1988– 1992.
- [21] G. Tabacchi, E. Fois, D. Barreca, A. Gasparotto, Phys. status solidi 2014, 211, 251-259.
- [22] G. Tabacchi, E. Fois, G. Calzaferri, Angen. Chemie Int. Ed. 2015, 54, 11112–11116.
- [23] C. Deiana, M. Fabbiani, G. Martra, M. Vincenti, M. Pazzi, Y. Sakhno, *ChemCatChem* **2013**, *5*, 2832–2834.
- [24] E. A. Carter, G. Ciccotti, J. T. Hynes, R. Kapral, Chem. Phys. Lett. 1989, 156, 472–477.
- [25] W. Humphrey, A. Dalke, K. Schulten, J. Mol. Graph. 1996, 14, 33–38.
- [26] M. Ceriotti, W. Fang, P. G. Kusalik, R. H. McKenzie, A. Michaelides, M. A. Morales, T. E. Markland, Chem. Rev. 2016, 116, 7529–7550.
- [27] M. E. Tuckerman, D. Marx, M. Parrinello, *Nature* 2002, 417, 925–929.
- [28] D. Jose, A. Datta, Angew. Chemie Int. Ed. 2012, 51, 9389-9392.
- [29] A. Fernández-Ramos, Angew. Chemie Int. Ed. 2013, 52, 8204–8205.
- [30] P. Durlak, Z. Latajka, J. Comput. Chem. 2019, 40, 671-687.
- [31] S. D. Ivanov, I. M. Grant, D. Marx, J. Chem. Phys. 2015, 143, 124304.
- [32] Y. Litman, D. Donadio, M. Ceriotti, M. Rossi, J. Chem. Phys. 2018, 148, DOI 10.1063/1.5002537.
- [33] M. Xu, H. Noei, M. Buchholz, M. Muhler, C. Wöll, Y. Wang, Catal. Today 2012, 182, 12–15.
- [34] C. Deiana, M. Minella, G. Tabacchi, V. Maurino, E. Fois, G. Martra, 2013, 15, 307–315.
- [35] A. Mattsson, L. Österlund, J. Phys. Chem. C 2010, 114, 14121–14132.
- [36] M. Fabbiani, M. Pazzi, M. Vincenti, G. Tabacchi, E. Fois, G. Martra, J. Nanosci. Nanotechnol. 2018, 18, 5854–5857.
- [37] D. C. Grinter, M. Nicotra, G. Thornton, J. Phys. Chem. C 2012, 116, 11643-11651.
- [38] R. F. W. Bader, Atoms in Molecules : A Quantum Theory, Clarendon Press, 1990.
- [39] R. F. W. Bader, Chem. Rev. 1991, 91, 893–928.
- [40] P. E. Blöchl, *Phys. Rev. B* **1994**, *50*, 17953–17979.
- [41] P. Giannozzi, S. Baroni, N. Bonini, M. Calandra, R. Car, C. Cavazzoni, D. Ceresoli, G. L. Chiarotti, M. Cococcioni, I. Dabo, et al., J. Phys. Condens. Matter 2009, 21, 395502.
- [42] W. Tang, E. Sanville, G. Henkelman, J. Phys. Condens. Matter 2009, 21, 084204.
- [43] G. Henkelman, A. Arnaldsson, H. Jó Nsson, n.d., DOI 10.1016/j.commatsci.2005.04.010.

- [44] M. Yu, D. R. Trinkle, J. Chem. Phys. 2011, 134, 64111.
- [45] A. O. F. Jones, M. H. Lemée-Cailleau, D. M. S. Martins, G. J. McIntyre, I. D. H. Oswald, C. R. Pulham, C. K. Spanswick, L. H. Thomas, C. C. Wilson, *Phys. Chem. Chem. Phys.* 2012, 14, 13273–13283.
- [46] F. Fontaine-Vive, M. R. Johnson, G. J. Kearley, J. A. K. Howard, S. F. Parker, J. Am. Chem. Soc. 2006, 128, 2963–2969.
- [47] F. Fontaine-Vive, M. R. Johnson, G. J. Kearley, J. A. Cowan, J. A. K. Howard, S. F. Parker, J. Chem. Phys. 2006, 124, 234503.
- [48] C. F. Matta, R. J. Boyd, in *Quantum Theory Atoms Mol.*, Wiley-VCH Verlag GmbH & Co. KGaA, Weinheim, Germany, n.d., pp. 1–34.